# Eddy-Induced Dispersion of Sea Ice Floes at the Marginal Ice Zone

Gupta, Mukund; Gürcan, Emma; Thompson, Andrew F.

**DOI**
10.1029/2023GL105656

**Publication date**
2024

**Document Version**
Final published version

**Published in**
Geophysical Research Letters

**Citation (APA)**
Gupta, M., Gürcan, E., & Thompson, A. F. (2024). Eddy-Induced Dispersion of Sea Ice Floes at the Marginal Ice Zone. *Geophysical Research Letters*, *51*(2), Article e2023GL105656. https://doi.org/10.1029/2023GL105656

**Important note**
To cite this publication, please use the final published version (if applicable).
Please check the document version above.

Geophysical Research Letters

RESEARCH LETTER
10.1029/2023GL105656

# Eddy-Induced Dispersion of Sea Ice Floes at the Marginal Ice Zone

**Mukund Gupta**[1,2], **Emma Gürcan**[1], **and Andrew F. Thompson**[1]

[1]California Institute of Technology, Pasadena, CA, USA, [2]Delft University of Technology, Delft, The Netherlands

**Key Points:**

- The sensitivity of sea ice dispersion and upper-ocean energetics to floe size is considered at a mesoscale front
- Floes smaller than turbulent filaments disperse more strongly and lead to a wider marginal ice zone
- These small floes allow for stronger eddy kinetic energy propagation and heat transport into the pack

**Supporting Information:**

Supporting Information may be found in the online version of this article.

**Correspondence to:**

M. Gupta,
guptam@caltech.edu

**Citation:**

Gupta, M., Gürcan, E., & Thompson, A. F. (2024). Eddy-induced dispersion of sea ice floes at the marginal ice zone. *Geophysical Research Letters*, *51*, e2023GL105656. https://doi.org/10.1029/2023GL105656

Received 27 JUL 2023
Accepted 13 DEC 2023

**Author Contributions:**

**Conceptualization:** Mukund Gupta, Andrew F. Thompson
**Formal analysis:** Mukund Gupta, Emma Gürcan
**Funding acquisition:** Andrew F. Thompson
**Investigation:** Mukund Gupta, Andrew F. Thompson
**Methodology:** Mukund Gupta
**Project Administration:** Andrew F. Thompson
**Resources:** Andrew F. Thompson
**Software:** Mukund Gupta
**Supervision:** Mukund Gupta, Andrew F. Thompson
**Validation:** Mukund Gupta



**Abstract** Ocean heat exchanges at the marginal ice zone (MIZ) play an important role in melting sea ice. Mixed-layer eddies transport heat and ice floes across the MIZ, facilitating the pack's access to warm waters. This study explores these frontal dynamics using disk-shaped floes coupled to an upper-ocean model simulating the sea ice edge. Numerical experiments reveal that small floes respond more strongly to fine-scale ocean currents, which favors higher dispersion rates and weakens sea ice drag onto the underlying ocean. Floes with radii smaller than resolved turbulent filaments (∼2–4 km) result in a wider and more energetic MIZ, by a factor of 70% each, compared to larger floes. We hypothesize that this floe size dependency may affect sea ice break-up by controlling oceanic energy propagation into the MIZ and modulate the sea ice pack's melt rate by regulating lateral heat transport toward the sea ice cover.

**Plain Language Summary** Sea ice forms as a thin layer of frozen ocean waters, which breaks into individual floes due to the action of waves, ocean currents, and atmospheric winds. At the edge of the pack, these floes are vulnerable to warm waters in the open ocean, which can favor the melt of sea ice. The transport of heat from the open ocean into ice-covered regions is not well represented in existing climate models, notably due to their poor spatial resolution and their inability to represent the dynamics of individual floes. In this study, we use a regional numerical model to investigate how fine-scale ocean currents (2–30 km) can help transport heat toward a sea ice pack composed of broken-up floes. We find that this heat transport is most efficient when floes are small, because they cannot efficiently damp the mechanical energy from the surface currents and they are easily transported into the open ocean by these currents. These two processes combined may lead to sea ice melt feedbacks that are currently not captured by coarser climate models.

## 1. Introduction

Marginal ice zones (MIZs) serve as transitional regions between the open ocean and the consolidated sea ice pack. MIZs are typically composed of relatively loose and thin ice that is susceptible to melt and breakage from the surrounding ocean and atmosphere, particularly in the summer months. Over the last decades, the width of the Arctic MIZ has increased by 10–20% (Rolph et al., 2020), coinciding with a loss of multi-year ice (Comiso, 2012), a thinning of the pack (Kwok & Rothrock, 2009) and increased sea ice drift speeds (Rampal et al., 2009). As the fraction of MIZ to total sea ice area continues to increase, the pack is likely to become weaker, more vulnerable to external forcings, and subject to stronger air-sea exchanges. Quantifying the climatic feedbacks associated with these evolving sea ice dynamics represents a challenge, with important ramifications for global-scale warming rates, ocean heat and carbon uptake, marine ecology, and operational forecasts in the rapidly changing polar environment (Kattsov et al., 2010).

Most climate models treat sea ice as a continuous fluid that can sustain internal stresses through a parameterized rheology representing floe-floe interactions within the pack. Sea ice rheology is typically calibrated to emulate basin-scale observations and relies on the assumption that the model grid size is much larger than individual floes. While internal stresses are relatively weak at the MIZ, the continuum approximation may lead to biases in sea ice melting rates and partly explain the mismatch between modeled and simulated concentration trends in these critical regions. The presence of loosely packed floes in the MIZ has motivated the development of discrete element models (DEMs), which can resolve interactions between ice floes forced by waves, ocean eddies and winds (Blockley et al., 2020; Damsgaard et al., 2018; Herman, 2016; Hopkins, 2004). DEMs have been used to simulate particles of varying geometrical complexity, including disks, polygons and more arbitrary shapes at scales ranging from several meters to tens of kilometers. The explicit representation of floes, with their complex size, thickness, and shape distributions has been shown to impact the ability of the pack to sustain internal stresses

**Visualization:** Mukund Gupta, Andrew F. Thompson
**Writing – original draft:** Mukund Gupta
**Writing – review & editing:** Mukund Gupta, Emma Gürcan, Andrew F. Thompson

(Manucharyan & Montemuro, 2022; West et al., 2022) and its melt rate during spring and summer (Gupta & Thompson, 2022; Moncada et al., 2023).

Climate models suggest that the mechanical response of the sea ice pack to ongoing thermodynamic melt in the Arctic Ocean will influence future rates of sea ice decline (Rampal et al., 2011). A thinner ice cover is prone to larger deformation rates, breakage and drift, which can enhance sea ice export through characteristic "choke points" in the Arctic Ocean, such as Fram Strait (Yang et al., 2023) and Nares Strait (Howell et al., 2023). Sea ice dispersion measured by tracked buoys exhibits distinct dynamical behaviors, ranging from a sub-diffusive regime characterized by important floe-floe interactions, to a super-diffusive regime, which describes floes drifting freely in response to winds and currents (Lukovich et al., 2015). Observations suggest that sea ice drift speeds have increased by approximately 10% per decade within the Arctic ocean from 1979 to 2007 (Rampal et al., 2009), which may signal ongoing or upcoming shifts in dispersion regimes manifesting at the basin scale. Larger drift velocities may also reduce the mean residence time of sea ice within the basin, which diminishes its ability to accumulate thickness over multiple years.

At the MIZ, the propagation of oceanic kinetic energy underneath the sea ice pack can break up floes and allow them to disperse into the surrounding open ocean. Surface waves can propagate up to 50 km into the Arctic and more than 100 km into the Antarctic sea ice cover, affecting sea ice breakage and motions over scales of 1–100 m (Thomson, 2022). At the mesoscale and sub-mesoscale (1–50 km), oceanic eddies influence the energetics of the MIZ and the size distribution of sea ice floes. Manucharyan and Thompson (2017) used a continuum sea ice model to show that in the absence of thermal feedbacks, cyclonic eddies located at the edge of the pack can trap and advect sea ice toward the warmer open ocean due to a combination of frictional and frontogenetic surface ocean convergence. Building on Horvat et al. (2016), Gupta and Thompson (2022) found that floe size can control the scale and strength of underlying mixed layer eddies, by influencing potential energy injection and kinetic energy dissipation associated with floe melt and ice/ocean friction, respectively. The geometrical properties of floes, such as their size distribution, are therefore also likely to influence sea ice dispersion rates into the warm open ocean, but those dependencies have not been quantified.

This study extends the work of Manucharyan and Thompson (2017) to investigate controls on MIZ width evolution using an eddying model of the upper ocean coupled to disk-shaped sea ice floes (Gupta & Thompson, 2022). We consider a regime consisting of the largest floes observed in the MIZ, several kilometers of diameter (Stern et al., 2018), which is comparable to the size of the smaller mesoscale eddies reported in the Arctic Ocean (Timmermans et al., 2008). For the same sea ice concentration, floes smaller than the characteristic eddy size dissipate less eddy kinetic energy (EKE) and disperse more readily than larger floes, resulting in a wider and more energetic MIZ. These feedbacks may play an important role in shaping upcoming sea ice changes over both hemispheres.

## 2. Model Description

This study makes use of the modeling framework outlined in Gupta and Thompson (2022), which consists of an upper-ocean model coupled to discrete element sea ice floes (Figure 1). The ocean model (Oceananigans.jl, Ramadhan et al., 2020) solves the non-hydrostatic Boussinesq equations on an $f$-plane with periodic boundary conditions in the $x$-direction and no normal flow with free slip boundary conditions in the $y$-direction. The model domain is 128 × 128 km in the horizontal with a resolution of 500 m; the vertical resolution varies between 1.25 and 14 m from the surface to 160 m depth. The model applies a biharmonic diffusivity in the horizontal ($\kappa_H = 1.5 \cdot 10^6$ m$^4$ s$^{-1}$) and a harmonic diffusivity in the vertical ($\kappa_V = 5 \cdot 10^{-5}$ m$^2$ s$^{-1}$). There is no bottom friction. The initial conditions consist of a quiescent summertime polar ocean with an idealized Arctic-like salinity-dominated stratification and temperature inversion in the vertical (Figure 1). There is a sharp density front in the mixed layer, delineating a cold and fresh region in the northern half of the domain and a relatively warm and salty region in the south. The northern region represents the MIZ, where we impose a fresh water lens of 25 m depth representing past sea ice melt. The southern half of the domain corresponds to the open ocean, where we impose a warm layer over the top 40 m, representing accumulated heat from solar heating (Timmermans & Marshall, 2020).

The sea ice model consists of disk-shaped floes, which respond to stresses imposed by surface ocean currents and inelastic collisions for both translational and rotational motion (Gupta & Thompson, 2022). We design a set of

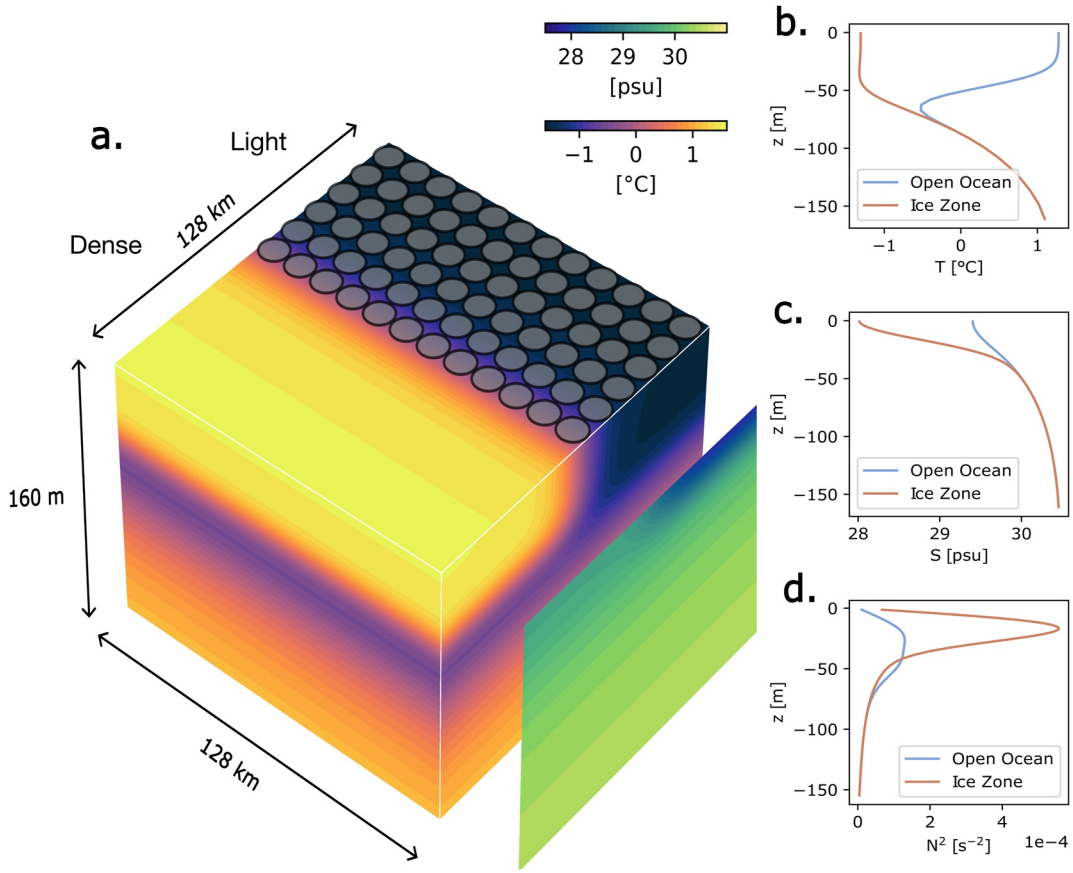


**Figure 1.** Initial conditions in the coupled ocean/sea ice floe model. (a) Mixed layer front characterized by cold and fresh waters in the marginal ice zone (covered by circular floes) and warm and salty waters at the surface of the open ocean. Horizontally averaged initial profiles of (b) temperature, (c) salinity, and (d) squared buoyancy frequency for the open ocean (blue) and ice covered region (orange), respectively.

simulations with floes characterized by a uniform radius $R_f$ varying between 2, 5, and 10 km (Rf2, Rf5, and Rf10), and a uniform thickness of 1.5 m. We consider floes that are either 2-way coupled to the ocean (2w), where ice/ocean stress affects the momentum of the ocean, or 1-way coupled (1w), where the ocean is unaffected by the presence of the floes. Additionally, we consider a simulation with a passive surface tracer (PST) in lieu of floes, which approximates the behavior of a highly fractured sea ice pack (i.e., much smaller floes) with negligible internal stresses and ice/ocean friction. The tracer responds to advection by the surface horizontal velocity and a horizontal harmonic diffusion of 10 $m^2\ s^{-1}$ chosen for numerical stability. All experiments start with approximately 68% sea ice (or tracer) concentration in the northern half of the domain. This concentration is evaluated over the ocean model grid by projecting the area of sea ice floes on to intersecting cells. Following Manucharyan and Thompson (2017), we do not consider the effects of winds or sea ice melt. The numerical experiments are run in a transient (non-equilibrated) configuration for 80 days, which corresponds approximately to the length of the melt season. The model constants are summarized in Table S1 in Supporting Information S1.

## 3. Results

### 3.1. Floe Size Influence on Lateral Exchanges Within the MIZ

In all simulations, a westward jet develops over the central part of the domain due to geostrophic adjustment at the front, since the surface ocean in the northern half of the domain is initially less dense and $f$ is positive (Figure 2). As the jet accelerates, baroclinic instability leads to the formation of eddies and filaments, which enhance the meridional transport of dense surface waters from the open ocean toward the sea ice zone. At the surface, these lateral exchanges carry sea ice floes toward the open ocean, while eddying motions spread both northward and

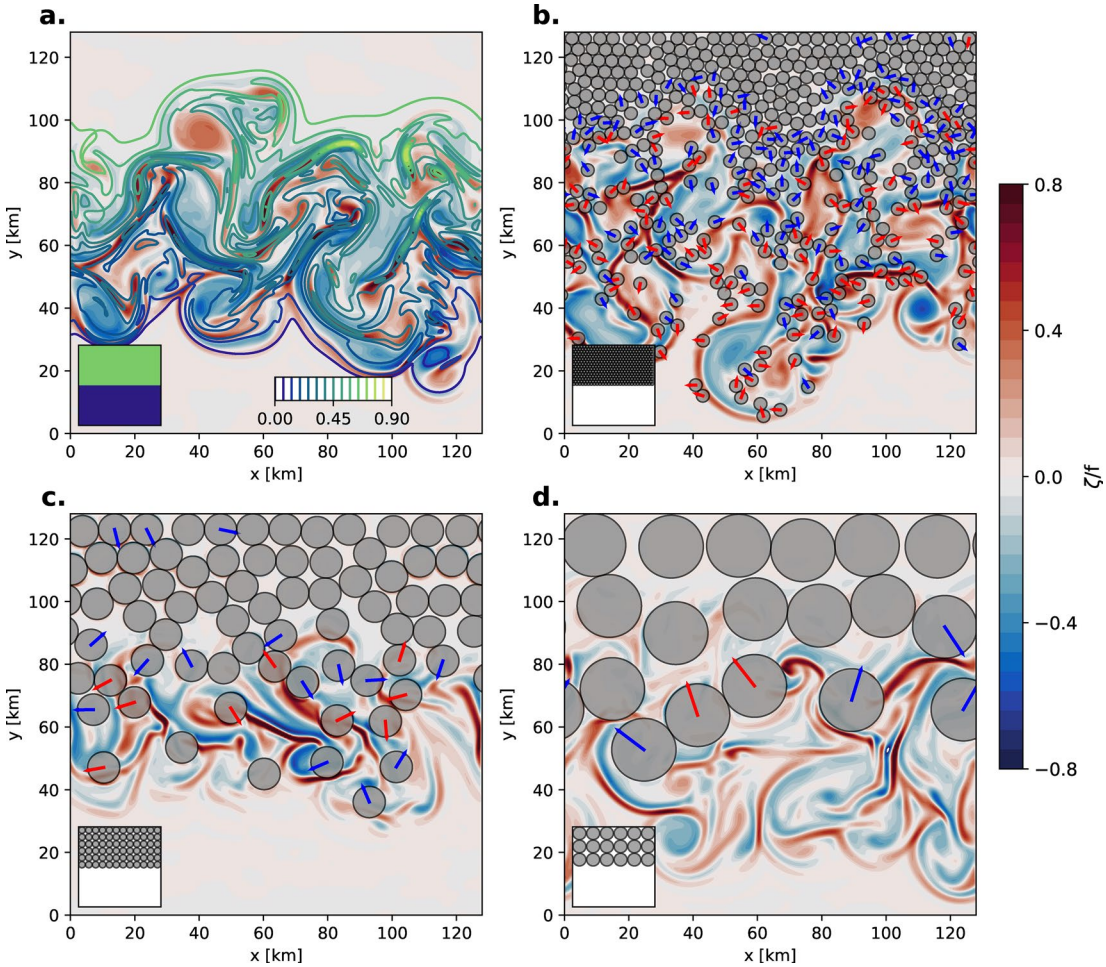


**Figure 2.** Snapshots of the normalized relative vorticity $\zeta/f$ at the ocean surface with overlaid representations of sea ice (disk-shaped floes) taken after 80 days of the following simulations: (a) passive surface tracer, (b) $R_f = 2$ km (2-way), (c) $R_f = 5$ km (2-way), and (d) $R_f = 10$ km (2-way). In panel (a), the colored lines represent contours of the tracer. In panels (b–d), the circles represent individual floes. Colored lines within floes indicate their orientation (set at 0° for the initial time step), and the sign of rotation (red: anticyclonic and blue: cyclonic). The orientation angle is only plotted if the rotation rate exceeds 0.1 day$^{-1}$. The insets at the bottom left of each panel represent the initial distribution of the passive tracer (panel (a)) or the starting position of floes (panels (b–d)).

southward from the central part of the domain. The mixed-layer baroclinic radius of deformation ($NH_m/f$) is 5 km, such that the smallest floes considered in our simulations ($R_f = 2$ km) are smaller than typical eddies, while the larger floes ($R_f = 5$, 10 km) are bigger or comparable to the eddy size. In what follows, we characterize the evolution of the MIZ width resulting from the dispersion of floes, the energetics of the upper ocean mediated by ice/ocean friction and the influence of floe size on the trapping of ice within filaments and eddies.

The cross-front dispersion of floes, and hence the evolution of the MIZ width, depends on floe size. Small floes ($R_f = 2$ km) disperse at a similar rate to the PST, since their motions respond to the finest eddy scales resolved by the simulations (Figures 3a and 3b). Larger floes ($R_f = 5$, 10 km) integrate the competing influences of several filaments and eddies, resulting in weaker ice motion and a narrower MIZ for both 1-way and 2-way coupled simulations. The size dependence of floe dispersion affects the oceanic heat content in direct contact with sea ice. The probability distribution function (PDF) of surface ocean temperature under ice in the MIZ displays a peak between −1.1°C and −0.7°C, along with a tail that extends to warmer temperatures, due to the dispersion of floes. Small floes ($R_f = 2$ km) and the tracer exhibit a similar PDF, with a higher mean and a wider tail, compared to the larger floes (Figure 3b). This temperature difference reflects the ability of floes with radii smaller than the characteristic filament size (~2–4 km) to drift readily into the open ocean and access its warmth through lateral heat exchanges.

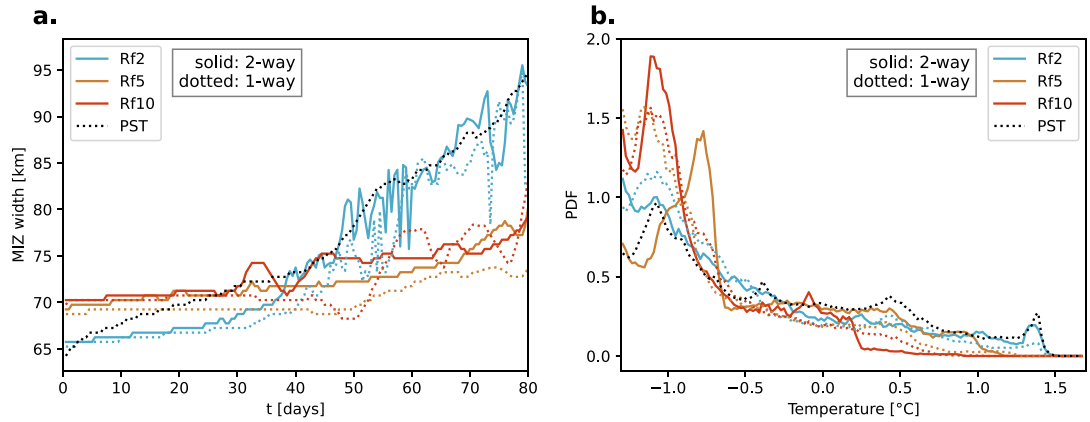


**Figure 3.** (a) Width of the marginal ice zone defined as the zonal-mean latitude of the 15% sea ice (or tracer) concentration contour. (b) Probability distribution function of the surface ocean temperature evaluated over grid cells that have a sea ice (or tracer) concentration greater than 5%. Grid cells with a surface temperature less than −1.3°C are not included in the distribution to avoid the contribution of floes that remain largely within the northern part of the domain.

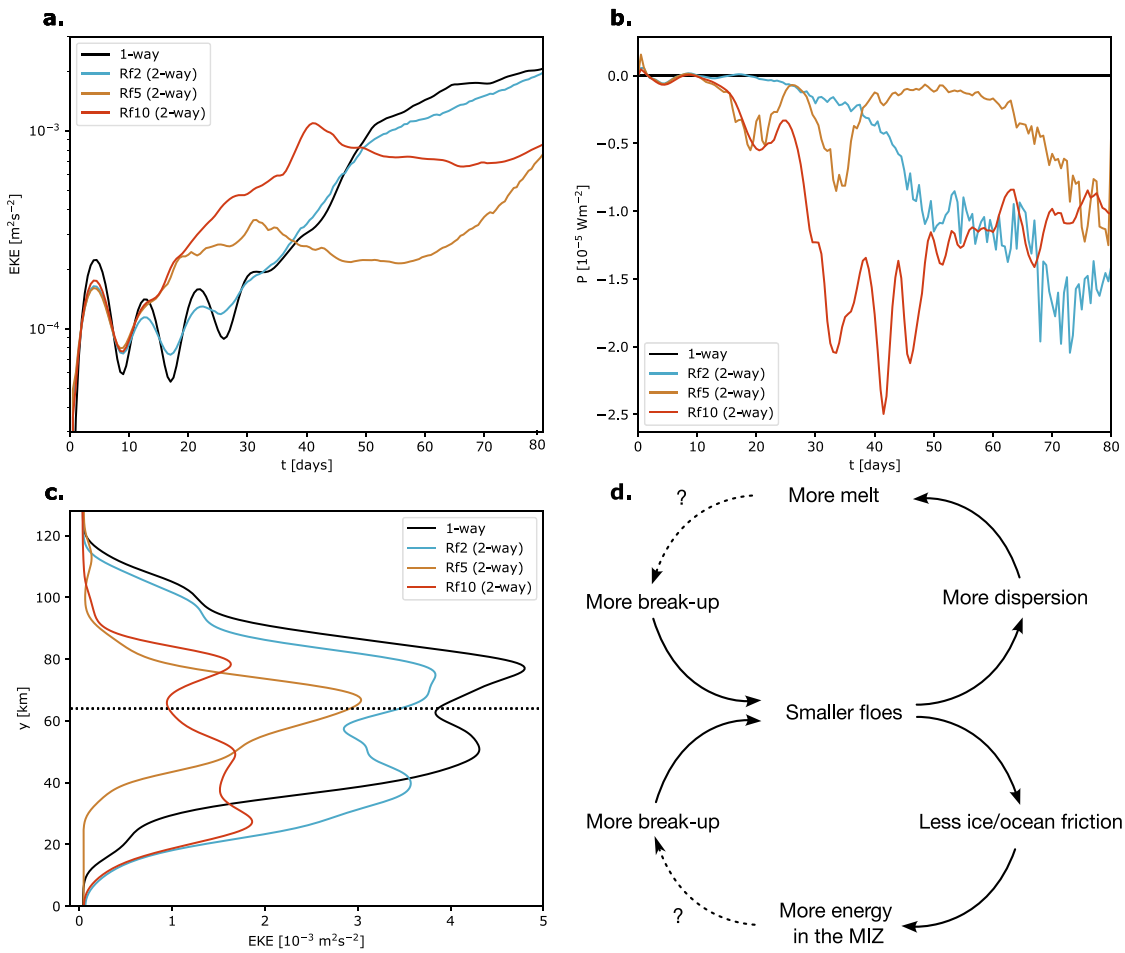


**Figure 4.** (a) Time evolution of horizontally-averaged surface eddy kinetic energy (EKE). (b) Time evolution of the horizontally-averaged power transfer from ocean to sea ice *P*. (c) Zonal-mean surface EKE averaged over the last 3 days of the simulation and smoothed by a Gaussian filter with a window of 1.5 km. The ocean behavior is the same for all 1-way coupled simulations. The dotted line marks the location of the meridional center of the domain. (d) Schematic illustrating potential positive feedbacks associated with floe size; dotted lines indicate more speculative components of the feedback mechanisms.

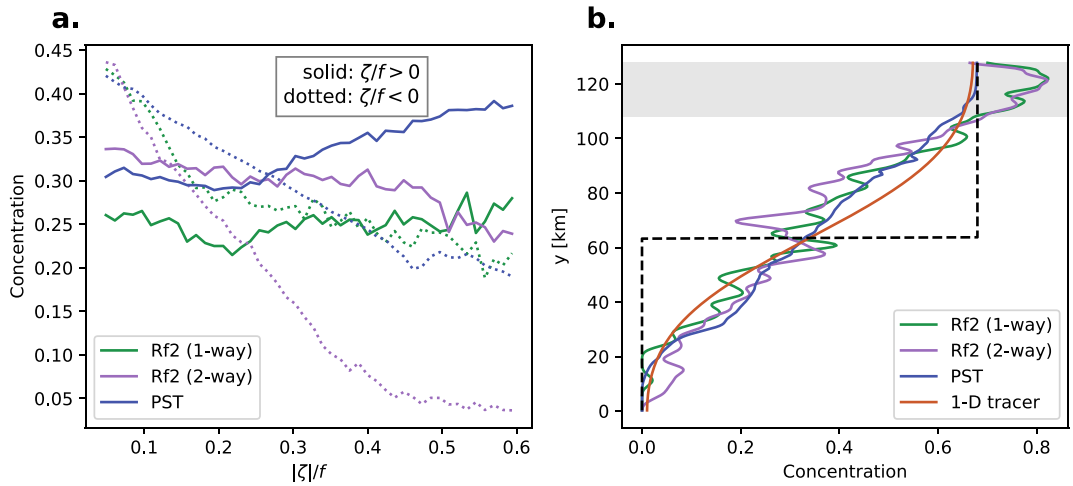


**Figure 5.** (a) Distribution of sea ice (or tracer) concentration evaluated over the last 10 days of the simulations and binned over the surface ocean's normalized relative vorticity ($\zeta/f > 0$: cyclonic and $\zeta/f < 0$: anticyclonic). (b) Zonal-mean sea ice (or tracer) concentration at the end of the simulations. The orange line shows the corresponding concentration from a 1-D diffusive model with prescribed diffusivity $\kappa = 50$ m$^2$ s$^{-1}$ and an initial concentration emulating the configuration of the numerical experiments, as shown in the black dotted line. The gray shading highlights the location experiencing up-gradient fluxes of sea ice concentration in Rf2-1w and Rf2-2w.

Ice-ocean coupling, mediated by floe size, also affects the time evolution of the ocean's surface EKE (Figure 4a). In the initial phase of eddy formation, EKE in experiments with 2-way coupled large floes (Rf5-2w and Rf10-2w) grows faster than for the 1-way coupled simulations, due to an instability associated with ice/ocean coupling (Figure S1 in Supporting Information S1). We note that under more realistic conditions, such as with coastal bathymetry and a surface wind stress, this mechanism may be masked by other instabilities in the upper ocean. In the later stage of large-floe simulations, the oceanic EKE growth weakens due to sea ice drag, which we quantify via the ice to ocean power transfer $P = \boldsymbol{\tau} \cdot \mathbf{u}$, a product of the ice/ocean stress $\boldsymbol{\tau}$ and the surface ocean velocity $\mathbf{u}$ (Figure 4b). The experiment containing 2-way coupled small floes (Rf2-2w) dissipates a smaller fraction of its oceanic kinetic energy, as small floes are more tightly coupled to both the translational and rotational motions imposed by surface currents (Gupta & Thompson, 2022).

The zonal-mean distribution of surface EKE illustrates the influence of floe size on the meridional propagation of oceanic energy within the sea ice pack (Figure 4c). For 1-way coupled simulations, the EKE distribution is mostly symmetric about the meridional center of the domain, as the ocean is not influenced by sea ice. Similarly, for Rf2-2w, the EKE distribution remains rather symmetric, as the ice/ocean stress is not large enough to strongly arrest the propagation of eddies within the pack. However, for Rf5-2w and Rf10-2w, the meridional EKE distribution is both smaller in magnitude and skewed toward the open ocean, reflecting the reduced propagation of oceanic energy within the pack due to sea ice damping. EKE production may also be altered by interactions with sea ice, but we do not quantify this effect here.

Taken together, the coupled eddy-floe interactions explored in this work may lead to feedbacks that can affect the evolution of the MIZ. Simulations with smaller floes ($Rf = 2$ km) have an MIZ that is roughly 70% broader and more energetic, compared to large-floe simulations ($Rf = 5$ and 10 km). The higher energy content of the MIZ and greater heat transport to the pack could favor subsequent break up of the pack into smaller floes (Figure 4d), but further work is required to explore this potential feedback and its climatic relevance.

### 3.2. Contrasting Small Floes With a Passive Surface Tracer

The domain-averaged sea ice dispersion of simulations with small floes (Rf2-1w and Rf2-2w) suggests that their behavior is akin to that of a PST (Figure 3). Here, we investigate whether this conclusion holds at the scale of individual floes and eddies.

We evaluate the ice trapping characteristics of ocean turbulent features by binning the sea ice and tracer concentrations according to the surface relative vorticity $\zeta/f$ for the PST, Rf2-1w, and Rf2-2w experiments (Figure 5a).

All simulations show an enhanced concentration distribution at weakly anticyclonic values (negative $\zeta/f$), which is due to slowly rotating floes on the cold side of the front (Figure 2). For higher magnitudes of $\zeta/f$, the tracer (PST) is preferentially trapped within cyclonic features, likely due to surface ocean convergence associated with the decay of cyclonic eddies and filaments (Figure S2 in Supporting Information S1). By contrast, with small floes and 1-way coupling (Rf2-1w), there is no enhancement of sea ice concentration within either cyclonic or anticyclonic eddies. This absence of trapping is a result of centripetal acceleration expelling floes out of regions of high vorticity magnitude, due to radial imbalance (Zhang et al., 2015). For 2-way coupled small floes (Rf2-2w), cyclonic trapping is active, due to ice/ocean drag promoting Ekman-induced surface convergence within cyclonic features (Manucharyan & Thompson, 2017).

Differences between resolved floes and the PST can also arise due to floe-floe interactions. In regions of low sea ice concentration, resolved floes disperse similarly to the PST and a 1-D tracer with prescribed diffusivity (Figure 5b and Figure S3 in Supporting Information S1). However, at the northern boundary, mechanical interactions between floes result in sea ice accumulation, which amounts to an up-gradient flux of concentration. This accumulation is aided by resolved floes sustaining compressive stresses, as eddies press them against the northern boundary. The resulting up-gradient flux is likely sensitive to the collision parameterization, and may be relevant for MIZ interactions with the compacted sea ice cover and continental boundaries.

## 4. Discussion and Conclusions

This study makes use of a model of upper-ocean turbulence coupled with circular sea ice floes to investigate mechanical ice-ocean interactions at a summer mixed-layer MIZ front. Eddy generation at the front promotes lateral heat exchanges at the sea ice edge and the widening of the MIZ extent due to floe dispersion. Floes smaller than the typical eddy size disperse more readily and dissipate less oceanic power than large floes, resulting in a wider, warmer and more energetic MIZ. In our simulations, this regime transition occurs around 2–4 km length scale, but this threshold may vary depending on regional eddy characteristics.

We hypothesize that the floe size dependence of MIZ dynamics could result in feedback loops affecting summertime sea ice melt rates (Figure 4d). Smaller floes allow more oceanic EKE to penetrate underneath the pack, which could promote further sea ice break up. Greater floe dispersion may also diminish the strength of the sea ice cover by allowing higher basal melt and reducing the areal concentration of sea ice floes, thus rendering the MIZ more prone to fracturing by waves (Thomson, 2022). These feedbacks may amplify the response of the pack to environmental changes (Manucharyan & Thompson, 2022), but their effect needs to be quantified in basin-wide simulations that account for realistic floe dynamics and consider variability over longer time scales.

The potential melt feedbacks associated with floe size depend on breakage and melt processes that are not included in the modeling framework of this study. Further work will benefit from explicitly modeling sea ice fractures using realistic floe geometries and size distributions, along with representations of thermodynamic melt and its effect on mixed layer eddies (Gupta & Thompson, 2022; Horvat et al., 2016). The strength of the positive melt feedbacks may also vary with sea ice concentration, as compacted ice can damp the surface expression of oceanic eddies (Gupta et al., 2020; Meneghello et al., 2021; Ou & Gordon, 1986). While the fundamental physical processes described in this study should be relevant in both polar regions, their aggregate affect may differ due to environmental conditions, such as the presence of larger floes in the Arctic (Roach et al., 2018), and frequent energetic storms in the Antarctic.

In the MIZ, continuum sea ice models only weakly dissipate oceanic EKE, due to small internal ice stresses at low ice concentrations. Our results suggest that if the MIZ contains floes of size comparable to oceanic eddies, the continuum approximation could overestimate its width and EKE content. However, this inference should be tested in DEMs that include breakage processes and realistic floe shapes. We also find that resolved floe-floe interactions can lead to up-gradient fluxes of sea ice concentration, due to eddies converging ice into more compact regions of the pack. These dynamics cannot be captured by a diffusion law, and likely depend on the details of the sea ice floe rheology. Assessing whether continuum sea ice parameterizations can reproduce the discrete element behaviors observed here is thus an important step in improving the representation of the MIZ within global climate models.

## Data Availability Statement

The sea ice floe code is provided in Gupta (2022), "Oceananigans.jl" is available in Ramadhan et al. (2020), and simulation data is stored in Gupta et al. (2023).

**Acknowledgments**
M.G., E.G., and A.F.T. were supported by the Office of Naval Research Multidisciplinary University Research Initiative (MURI) on Mathematics and Data Science for Physical Modeling and Prediction of Sea Ice. A.F.T. also acknowledges support from the NSF OCE 1829969 Grant. The authors are grateful to two anonymous reviewers, whose insightful comments helped improve the manuscript.

## References

Blockley, E., Vancoppenolle, M., Hunke, E., Bitz, C., Feltham, D., Lemieux, J.-F., et al. (2020). The future of sea ice modeling: Where do we go from here? *Bulletin of the American Meteorological Society*, *101*(8), E1304–E1311. https://doi.org/10.1175/BAMS-D-20-0073.1

Comiso, J. C. (2012). Large decadal decline of the arctic multiyear ice cover. *Journal of Climate*, *25*(4), 1176–1193. https://doi.org/10.1175/JCLI-D-11-00113.1

Damsgaard, A., Adcroft, A., & Sergienko, O. (2018). Application of discrete element methods to approximate sea ice dynamics. *Journal of Advances in Modeling Earth Systems*, *10*(9), 2228–2244. https://doi.org/10.1029/2018MS001299

Gupta, M. (2022). Sea ice circular floe code [Software]. Zenodo. https://doi.org/10.5281/zenodo.6578706

Gupta, M., Gürcan, E., & Thompson, A. F. (2023). Simulation data for 'eddy-induced dispersion of sea ice floes at the marginal ice zone' [Dataset]. Zenodo. https://doi.org/10.5281/zenodo.8190251

Gupta, M., Marshall, J., Song, H., Campin, J.-M., & Meneghello, G. (2020). Sea-ice melt driven by ice-ocean stresses on the mesoscale. *Journal of Geophysical Research: Oceans*, *125*(11), e2020JC016404. https://doi.org/10.1029/2020JC016404

Gupta, M., & Thompson, A. F. (2022). Regimes of sea-ice floe melt: Ice-ocean coupling at the submesoscales. *Journal of Geophysical Research: Oceans*, *127*(9), e2022JC018894. https://doi.org/10.1029/2022JC018894

Herman, A. (2016). Discrete-element bonded-particle sea ice model design, version 1.3a – Model description and implementation. *Geoscientific Model Development*, *9*(3), 1219–1241. https://doi.org/10.5194/gmd-9-1219-2016

Hopkins, M. A. (2004). A discrete element Lagrangian sea ice model. *Engineering Computations*, *21*(2/3/4), 409–421. https://doi.org/10.1108/02644400410519857

Horvat, C., Tziperman, E., & Campin, J.-M. (2016). Interaction of sea ice floe size, ocean eddies, and sea ice melting. *Geophysical Research Letters*, *43*(15), 8083–8090. https://doi.org/10.1002/2016GL069742

Howell, S. E. L., Babb, D. G., Landy, J. C., Moore, G. W. K., Montpetit, B., & Brady, M. (2023). A comparison of Arctic Ocean sea ice export between nares strait and the Canadian Arctic archipelago. *Journal of Geophysical Research: Oceans*, *128*(4), e2023JC019687. https://doi.org/10.1029/2023JC019687

Kattsov, V. M., Ryabinin, V. E., Overland, J. E., Serreze, M. C., Visbeck, M., Walsh, J. E., et al. (2010). Arctic sea-ice change: A grand challenge of climate science. *Journal of Glaciology*, *56*(200), 1115–1121. https://doi.org/10.3189/002214311796406176

Kwok, R., & Rothrock, D. A. (2009). Decline in arctic sea ice thickness from submarine and ICESAT records: 1958–2008. *Geophysical Research Letters*, *36*(15), L15501. https://doi.org/10.1029/2009GL039035

Lukovich, J., Hutchings, J., & Barber, D. (2015). On sea-ice dynamical regimes in the Arctic Ocean. *Annals of Glaciology*, *56*(69), 323–331. https://doi.org/10.3189/2015AoG69A606

Manucharyan, G. E., & Montemuro, B. P. (2022). Subzero: A sea ice model with an explicit representation of the floe life cycle. *Journal of Advances in Modeling Earth Systems*, *14*(12), e2022MS003247. https://doi.org/10.1029/2022MS003247

Manucharyan, G. E., & Thompson, A. F. (2017). Submesoscale sea ice-ocean interactions in marginal ice zones. *Journal of Geophysical Research: Oceans*, *122*(12), 9455–9475. https://doi.org/10.1002/2017JC012895

Manucharyan, G. E., & Thompson, A. F. (2022). Heavy footprints of upper-ocean eddies on weakened arctic sea ice in marginal ice zones. *Nature Communications*, *13*(1), 2147. https://doi.org/10.1038/s41467-022-29663-0

Meneghello, G., Marshall, J., Lique, C., Isachsen, P. E., Doddridge, E., Campin, J.-M., et al. (2021). Genesis and decay of mesoscale baroclinic eddies in the seasonally ice-covered interior arctic ocean. *Journal of Physical Oceanography*, *51*(1), 115–129. https://doi.org/10.1175/JPO-D-20-0054.1

Moncada, R., Gupta, M., Thompson, A., & Andrade, J. E. (2023). Level set discrete element method for modeling sea ice floes. *Computer Methods in Applied Mechanics and Engineering*, *406*, 115891. https://doi.org/10.1016/j.cma.2023.115891

Ou, H. W., & Gordon, A. L. (1986). Spin-down of baroclinic eddies under sea ice. *Journal of Geophysical Research*, *91*(C6), 7623–7630. https://doi.org/10.1029/jc091ic06p07623

Ramadhan, A., Wagner, G. L., Hill, C., Campin, J.-M., Churavy, V., Besard, T., et al. (2020). Oceananigans.jl: Fast and friendly geophysical fluid dynamics on GPUS. *Journal of Open Source Software*, *5*(53), 2018. https://doi.org/10.21105/joss.02018

Rampal, P., Weiss, J., Dubois, C., & Campin, J.-M. (2011). IPCC climate models do not capture arctic sea ice drift acceleration: Consequences in terms of projected sea ice thinning and decline. *Journal of Geophysical Research*, *116*(C8), C00D07. https://doi.org/10.1029/2011JC007110

Rampal, P., Weiss, J., & Marsan, D. (2009). Positive trend in the mean speed and deformation rate of Arctic Sea ice, 1979–2007. *Journal of Geophysical Research*, *114*(C5), C05013. https://doi.org/10.1029/2008JC005066

Roach, L. A., Horvat, C., Dean, S. M., & Bitz, C. M. (2018). An emergent sea ice floe size distribution in a global coupled ocean-sea ice model. *Journal of Geophysical Research: Oceans*, *123*(6), 4322–4337. https://doi.org/10.1029/2017JC013692

Rolph, R. J., Feltham, D. L., & Schröder, D. (2020). Changes of the arctic marginal ice zone during the satellite era. *The Cryosphere*, *14*(6), 1971–1984. https://doi.org/10.5194/tc-14-1971-2020

Stern, H. L., Schweiger, A. J., Zhang, J., & Steele, M. (2018). On reconciling disparate studies of the sea-ice floe size distribution. *Elementa: Science of the Anthropocene*, *6*, 49. https://doi.org/10.1525/elementa.304

Thomson, J. (2022). Wave propagation in the marginal ice zone: Connections and feedback mechanisms within the air–ice–ocean system. *Philosophical Transactions of the Royal Society A: Mathematical, Physical & Engineering Sciences*, *380*(2235), 20210251. https://doi.org/10.1098/rsta.2021.0251

Timmermans, M.-L., & Marshall, J. (2020). Understanding Arctic Ocean circulation: A review of ocean dynamics in a changing climate. *Journal of Geophysical Research: Oceans*, *125*(4), e2018JC014378. https://doi.org/10.1029/2018JC014378

Timmermans, M.-L., Toole, J., Proshutinsky, A., Krishfield, R., & Plueddemann, A. (2008). Eddies in the Canada basin, Arctic Ocean, observed from ice-tethered profilers. *Journal of Physical Oceanography*, *38*(1), 133–145. https://doi.org/10.1175/2007JPO3782.1

West, B., O'Connor, D., Parno, M., Krackow, M., & Polashenski, C. (2022). Bonded discrete element simulations of sea ice with non-local failure: Applications to nares strait. *Journal of Advances in Modeling Earth Systems*, *14*(6), e2021MS002614. https://doi.org/10.1029/2021MS002614

Yang, Y., Min, C., Luo, H., Kauker, F., Ricker, R., & Yang, Q. (2023). The evolution of the Fram Strait sea ice volume export decomposed by age: Estimating with parameter-optimized sea ice-ocean model outputs. *Environmental Research Letters*, *18*(1), 014029. https://doi.org/10.1088/1748-9326/acaf3b

Zhang, W.-Z., Xue, H., Chai, F., & Ni, Q. (2015). Dynamical processes within an anticyclonic eddy revealed from Argo floats. *Geophysical Research Letters*, *42*(7), 2342–2350. https://doi.org/10.1002/2015GL063120